ELSEVIER

Materials Science and Engineering A 392 (2005) 209–221

MATERIALS SCIENCE & ENGINEERING A

www.elsevier.com/locate/msea

Recrystallization of oligocrystalline tantalum deformed by cold rolling

H.R.Z. Sandim[a,*], J.P. Martins[a], A.L. Pinto[b], A.F. Padilha[c]

[a] *Departamento de Engenharia de Materiais, FAENQUIL, P.O. Box 116, Lorena, SP 12600-970, Brazil*
[b] *Instituto Militar de Engenharia, IME, Rio de Janeiro 22290-270, Brazil*
[c] *Departamento de Engenharia Metalúrgica e de Materiais, Escola Politécnica, USP, São Paulo 05508-900, Brazil*

Received 29 October 2003; received in revised form 10 September 2004; accepted 15 September 2004

Abstract

The recrystallization behavior of coarse-grained tantalum deformed at large strains is strongly dependent on its deformation microstructure. In this regard, a longitudinal section of a high-purity coarse-grained tantalum ingot obtained by double electron-beam melting (EBM) was straight cold rolled to thickness reductions varying from 70 to 92% followed by annealing in vacuum at 900 and 1200 °C for 1 h. Microstructural characterization was performed in cold rolled and annealed specimens using scanning electron microscopy (SEM) in the backscattered mode (BSE), electron backscattered diffraction (EBSD), and microhardness testing. The recrystallization of individual grains is strongly dependent on their initial orientation. Recrystallization kinetics varies noticeably from one grain to another. Even after annealing at 1200 °C for 1 h, the microstructure of tantalum sections deformed to 92% predominantly consists of alternating bands of recrystallized grains with distinct size distributions and a few elongated areas marking the presence of individual grains softened by recovery. Results also show inhomogeneous in-grain and grain-to-grain spatial distributions of textures in the rolling plane.

Keywords: Tantalum; Oligocrystals; Recrystallization; Recovery; Texture; EBSD

1. Introduction

Tantalum has a body-centered cubic (b.c.c.) crystal structure and displays an unique combination of physical and chemical properties like a very high melting point (2998 °C), outstanding corrosion resistance, and high ductility even at cryogenic temperatures. Tantalum and its alloys have many applications including the manufacture of equipments for chemical processing plants, and devices for electronic, aerospace and military industries [1].

Electron-beam melting (EBM) is the most suitable technique to produce high-purity tantalum because of its enhanced refining capability. Interstitial impurities such as oxygen and nitrogen must be minimized (O <150 wt-ppm and N <100 wt-ppm)[1] to ensure high ductility and avoiding embrittlement in tantalum. Electron-beam melting provides these requirements. The microstructure of high-purity tantalum EBM ingots consists of a few coarse columnar grains whose grain boundaries are almost parallel to the longitudinal ingot axis. The grain size of electron-beam melted tantalum ingots is commonly in the cm-range. A similar grain structure is found in VAR (vacuum arc remelting) ingots.

Following EBM, conventional deformation processes like rolling and swaging are carried out to get tantalum plates, sheets, rods, and other semi-finished products. Cold working is the preferred fabrication method to produce semi-finished products because of tantalum's poor oxidation resistance and high affinity for interstitials at elevated temperatures.

There are several reasons to use high-purity tantalum oligocrystals to investigate orientation effects on recrystallization. First, because of its high purity, solute drag effects on boundary migration during annealing are minimized. Second, individual grains can be traced during deformation and further static annealing easing the comparison of their behaviors. Third, the identification of the initial grains nucleated at deformation heterogeneities and grain boundary regions is easier in oligocrystals especially when annealing is performed at low homologous temperatures (e.g. 700–900 °C).

* Corresponding author. Tel.: +55 12 3159 9916; fax: +55 12 3153 3006.
E-mail address: hsandim@demar.faenquil.br (H.R.Z. Sandim).

[1] Chemical requirements specified in ASTM B-364-92.

0921-5093/$ – see front matter © 2004 Elsevier B.V. All rights reserved.
doi:10.1016/j.msea.2004.09.032

The nature of the cold-worked state determines the annealing behavior in metals. In an earlier investigation [2], the recrystallization of coarse-grained tantalum deformed by cold swaging was found to be very inhomogeneous. The microstructure observed in the annealed state was very heterogeneous compared to the larger homogeneity found in fine-grained tantalum. Individual grains did behave quite differently during cold swaging displaying distinct deformation microstructures and work-hardening behaviors. Commonly found in coarse-grained materials are deformation heterogeneities like deformation and shear bands. These heterogeneities contribute to increased differences in terms of stored energy and act as preferential nucleation sites for recrystallization.[3,4]. As a result, grain size and recrystallized volume fraction varied significantly from one grain to another. Hence, banded grains are expected to display a heterogeneous behavior regarding further recovery and recrystallization [5]. In the present paper, a coarse-grained tantalum slab was straight cold rolled to large strains and annealed at 900 and 1200 °C in order to obtain distinct microstructures in terms of recrystallized fraction. This work reports the development of in-grain and grain-to-grain texture gradients in the rolling plane of oligocrystalline tantalum.

2. Experimental

The starting material was a 78 mm diameter ingot obtained by means of double electron-beam melting of tantalum scrap. Table 1 presents the chemical composition of this ingot. The impurity contents are in agreement with ASTM-B-364-92. A 10 mm thick slab was carefully cut out from the ingot and straight cold rolled in multiple passes to 92% thickness reduction without intermediary annealing. In every part of this article, RD represents the rolling direction, TD the transverse direction, and ND the normal direction of the rolled sheet. Specimens in the deformed state (70, 80, and 92% reductions) were cut out parallel to the RD and vacuum-sealed in quartz glass. Three consecutive strips (10 mm wide) containing at least five bicrystals each were sampled from the rolled plate after every reduction. The prior grain boundaries (referred to the as-cast condition) were aligned nearly parallel to the RD. Fig. 1 shows a schematic representation of the sampling procedure adopted in the present work. One strip was used for investigating the as-rolled structure. The two remaining strips were annealed at 900 and 1200 °C for 1 h in vacuum. Selected bicrystals were cut from these strips for metallographic inspection. Vickers hardness tests were carried out in deformed and annealed specimens using a load of 100 g. Fifteen determinations were made on each specimen. Channeling contrast images of selected regions were obtained in a LEO 1450-VP scanning electron microscope operating at 30 kV. The EBSD scans were carried out in the rolling plane with mapped areas varying according to the magnification. EBSD sampling points were spaced from 8 to 20 μm for the annealed specimens (corresponding to the map step size). Microtexture evaluation (pole figures, inverse pole figures and orientation distribution function (ODF)) was determined by means of automatic indexing of Kikuchi patterns after suitable image processing in a TSL 3.0 system interfaced to a Philips XL-30 SEM operating at 20 kV with a conventional W-filament.

Table 1
Chemical composition of the EBM-Ta ingot used in this investigation

Impurity	Content (wt-ppm)
W	<55
Fe	<45
Al	<30
Si	<50
N	5 ± 3
O	65 ± 10
Ta	Balance

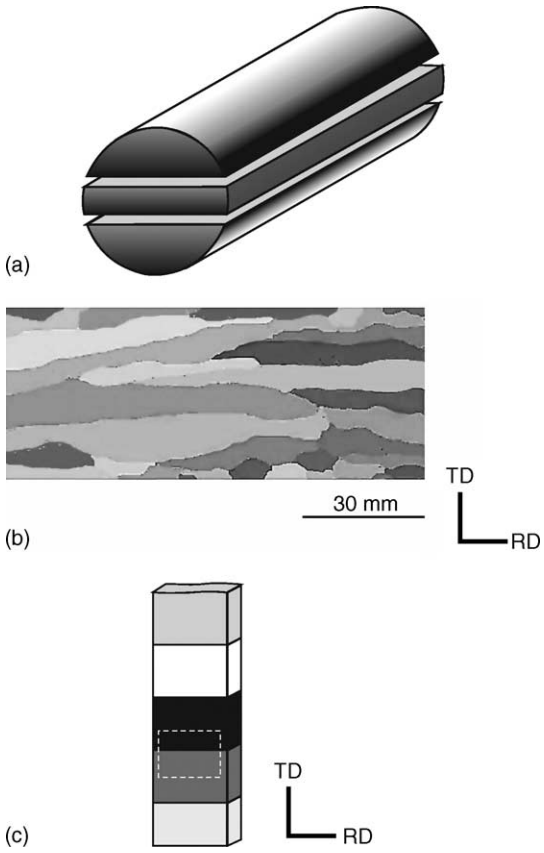

Fig. 1. Sampling procedure used in the present work: (a) sectioning of the tantalum slab prior to cold rolling; (b) longitudinal section showing the grain structure in the as-cast slab lying parallel to the RD. The dashed area in (c) corresponds to a typical example of a bicrystal sampled in the rolled plate.

3. Results

3.1. Starting material

The microstructure of the tantalum ingot consisted of coarse elongated grains with 40 mm in length and 10 mm in

width. Some grains in the central part of the ingot were up to 150 mm in length. These grains are nearly parallel to the longitudinal direction. The aspect ratio of the grains in the longitudinal section was about 5. Fig. 1b shows the longitudinal section of the EBM-Ta ingot used in this investigation. From a practical viewpoint, the slab cut from the tantalum ingot consisted of only a few coarse-elongated grains arranged in parallel. The initial thickness of the slab corresponds to the size of the individual grains. The hardness in as-cast tantalum was found to be 66 ± 5 (VHN, 5 kg). The orientation of individual grains in the slab was not determined in the present work.

3.2. Deformed specimens

Pure tantalum is very ductile and can be rolled to very large strains at room temperature. The microstructure of the longitudinal sections of cold deformed specimens is very inhomogeneous. The nature of the substructure developed varied significantly from one grain to another. Fig. 2 shows the two neighboring grains in 70% cold-rolled tantalum [6]. While grain A appeared structureless in SEM (electron channeling contrast), grain B has been subdivided in a much finer substructure. These distinct subdivision patterns were confirmed by EBSD measurements. The distributions of the misorientations (ψ) found in each grain are schematically shown in Fig. 2. Grain B has subdivided in a wide range of misorientations with many boundaries having high angle character ($\psi > 15^\circ$). On the other hand, the misorientation distribution shows that low angle boundaries are predominant in grain A ($\psi < 8^\circ$).

In-grain microstructural inhomogeneities are also found in cold-rolled tantalum. Deformation heterogeneities are ob-

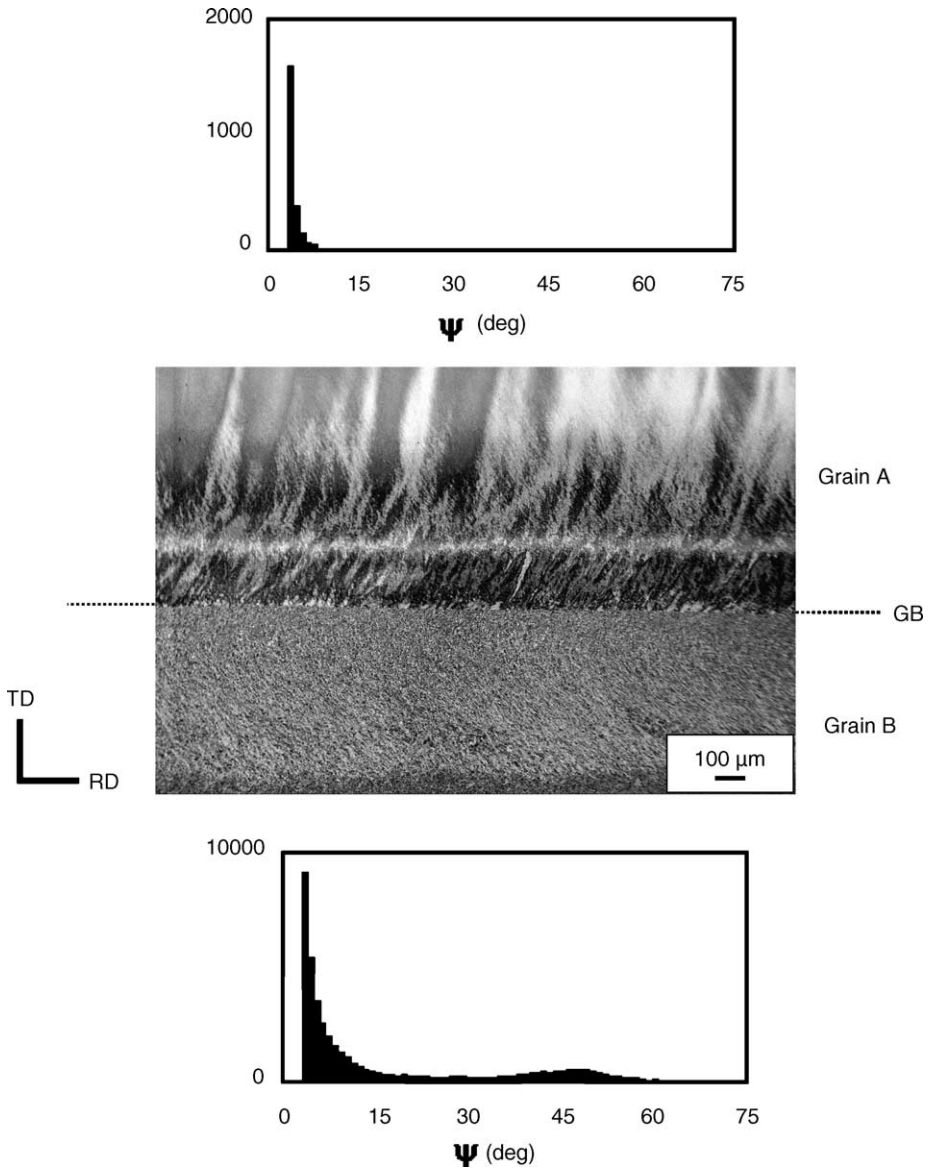

Fig. 2. Longitudinal section of grains A and B in 70% cold-rolled tantalum (SEM, BSE). Histograms showing the distribution of misorientations (ψ) measured in longitudinal section of grains A and B. The grain boundary referred to as-cast structure is indicated [6].

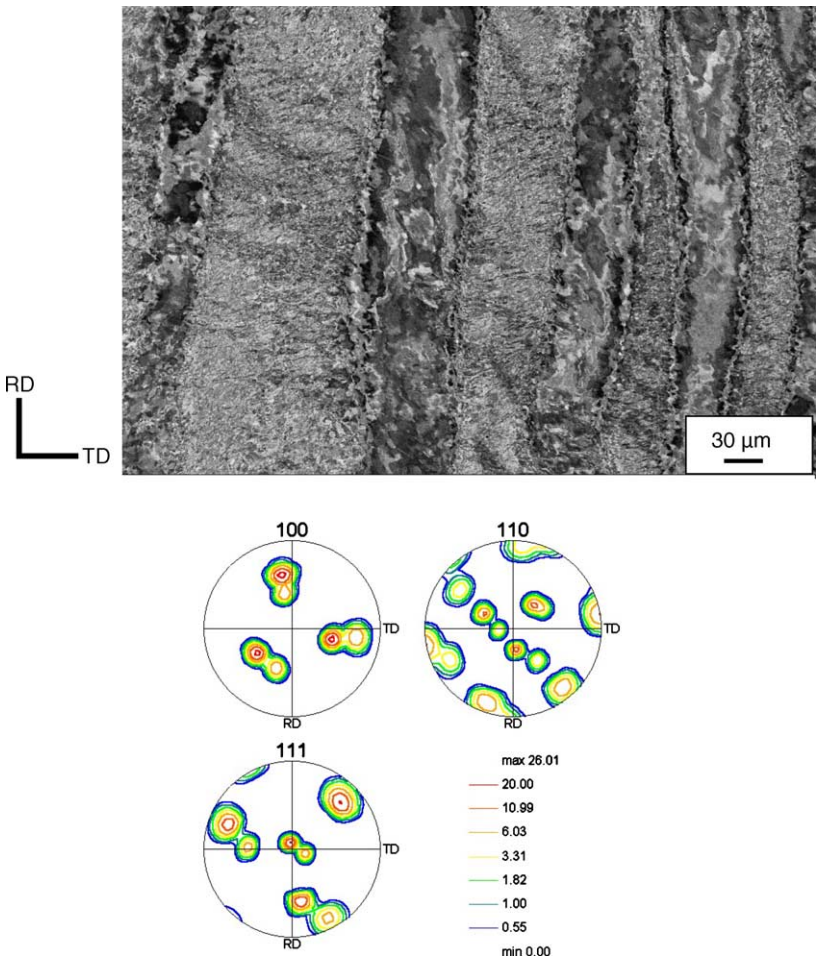

Fig. 3. SEM micrograph showing deformation bands subdividing a single grain in 70% cold-rolled EBM tantalum and corresponding pole figures indicating the orientation spread associated to banding.

served in most of the grains. Fig. 3 shows the presence of a banded structure developed within a single coarse grain. The corresponding pole figures show the orientation spread associated with the deformation bands. Deformation bands result from the fragmentation of unstable grains into regions of common orientations separated by narrow transition bands (geometrically necessary boundaries). These regions deform uniformly but with different combinations of slip systems. Large orientation changes are found across these bands. The tendency of grains for banding can be related to size and orientation effects [7]. In the following section, further examples of microstructural heterogeneity will be presented in selected bicrystals during annealing.

3.3. Annealed microstructures

During annealing, both recovery and recrystallization kinetics are very inhomogeneous in cold-rolled tantalum. Fig. 4 shows the microstructure of grains A and B after annealing at 1200 °C for 1 h. Recovery was predominant in grain A whereas grain B was fully recrystallized. EBSD investigation in the annealed state confirms that grain A is about 15°-$\{0\,0\,1\}\langle 1\,1\,0\rangle$-oriented (rotated cube). Very coarse grains growing towards grain A are also found. $\{1\,1\,0\}$-pole figures corresponding to these grains and to the recovered grain A are also shown. Fig. 5a shows the orientation image mapping (OIM) of the recrystallized structure shown in Fig. 4. In this figure, it is evident that grain size varies in the recrystallized structure. Pole figures (see Fig. 5c) show the orientation of fine (left side of the OIM) and coarse-elongated (right side of the OIM) grains in the former grain boundary region. There are no significant changes in texture from one region to another.

Fig. 6 shows another example of how inhomogeneous the annealing behavior is of two adjacent grains in the rolled plate. The bicrystal shown in this micrograph consists of grains E and F. The substructure of both grains is quite different (Fig. 6a). Grain E is subdivided in a finer subgrain structure. Measured Vickers microhardness values confirm these differences in terms of the developed substructure in both grains (Table 2). In consequence, grain E recrystallized in full extent whereas grain F was softened by recovery after annealing at 1200 °C for 1 h (Fig. 6b). Table 2 shows the results of Vickers microhardness testing

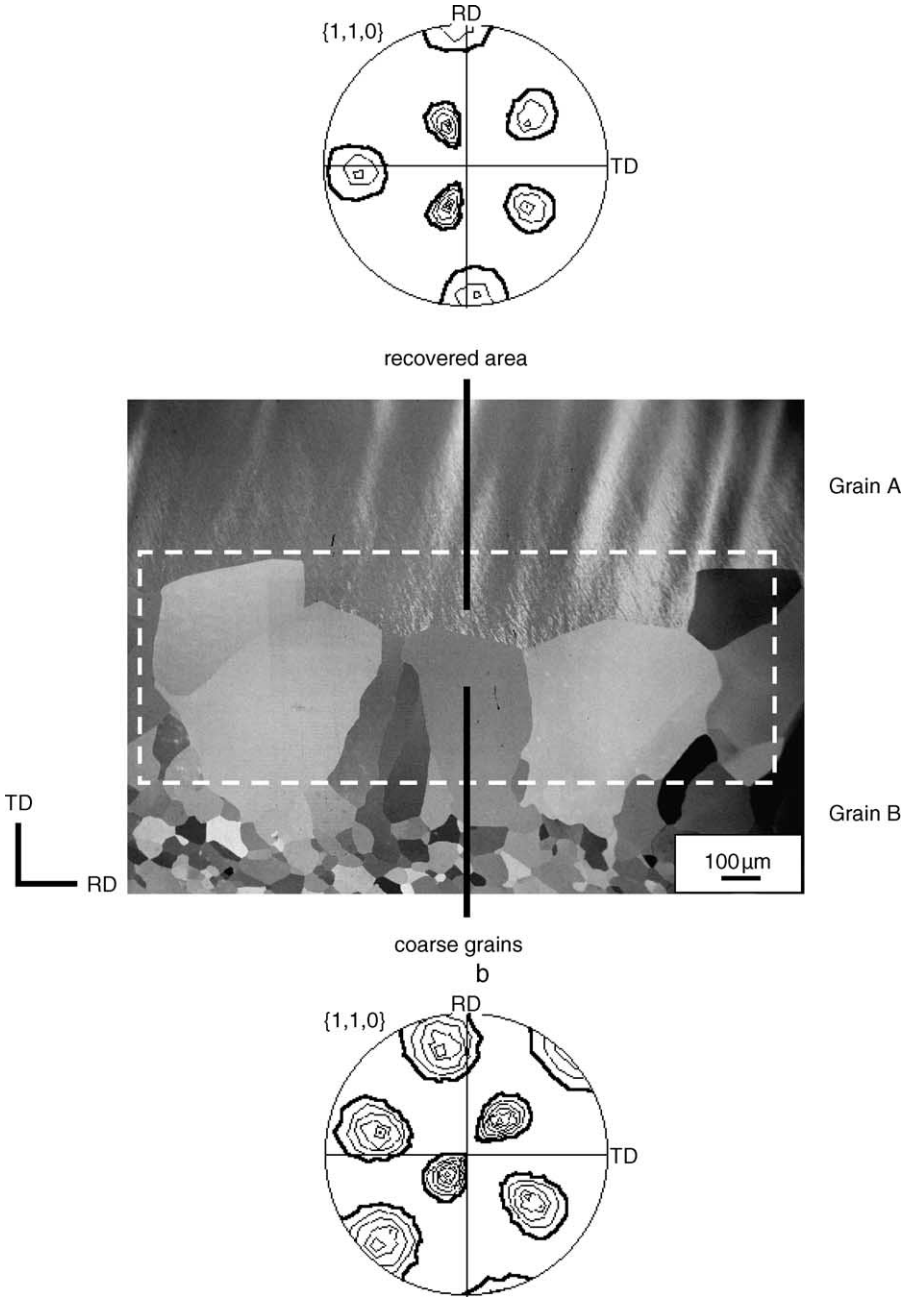

Fig. 4. Longitudinal section of the former bicrystal formed by grains A and B (referred to Fig. 2) after 70% cold rolling followed by annealing at 1200 °C for 1 h (SEM, BSE). Note large grains growing towards grain A and a fine equiaxed structure at the lower part of the micrograph [6]. {1 1 0}-pole figures corresponding to the recovered region and to the coarse-elongated grains are also shown.

for other grains and their corresponding annealing behaviors.

Another example of microstructural heterogeneity in tantalum is shown in Fig. 7. This figure shows three consecutive grains identified as G, H, and I. Grain H is positioned between grains G and I and did not undergo recrystallization upon annealing. On the other hand, grains G and I did recrystallize in full extent when annealed at 1200 °C for 1 h. The presence of coarse-elongated grains growing towards grain H is similar to those observed in Fig. 4. It is plausible to admit that longer annealing times could lead to a full recrystallized structure, however, nucleation appears to be absent in grain H.

Orientation effects are also evident in Fig. 8. Two neighbor grains display distinct annealing behaviors even after 92% reduction followed by annealing at 1200 °C for 1 h. Fig. 8a shows the SEM micrograph of this particular region. The strong microtexture developed in the recrystallized region (lower part of this micrograph) is $\{1\,1\,1\}\langle 1\,1\,2\rangle$ (a γ fiber component). The recovered region (upper part of the micro-

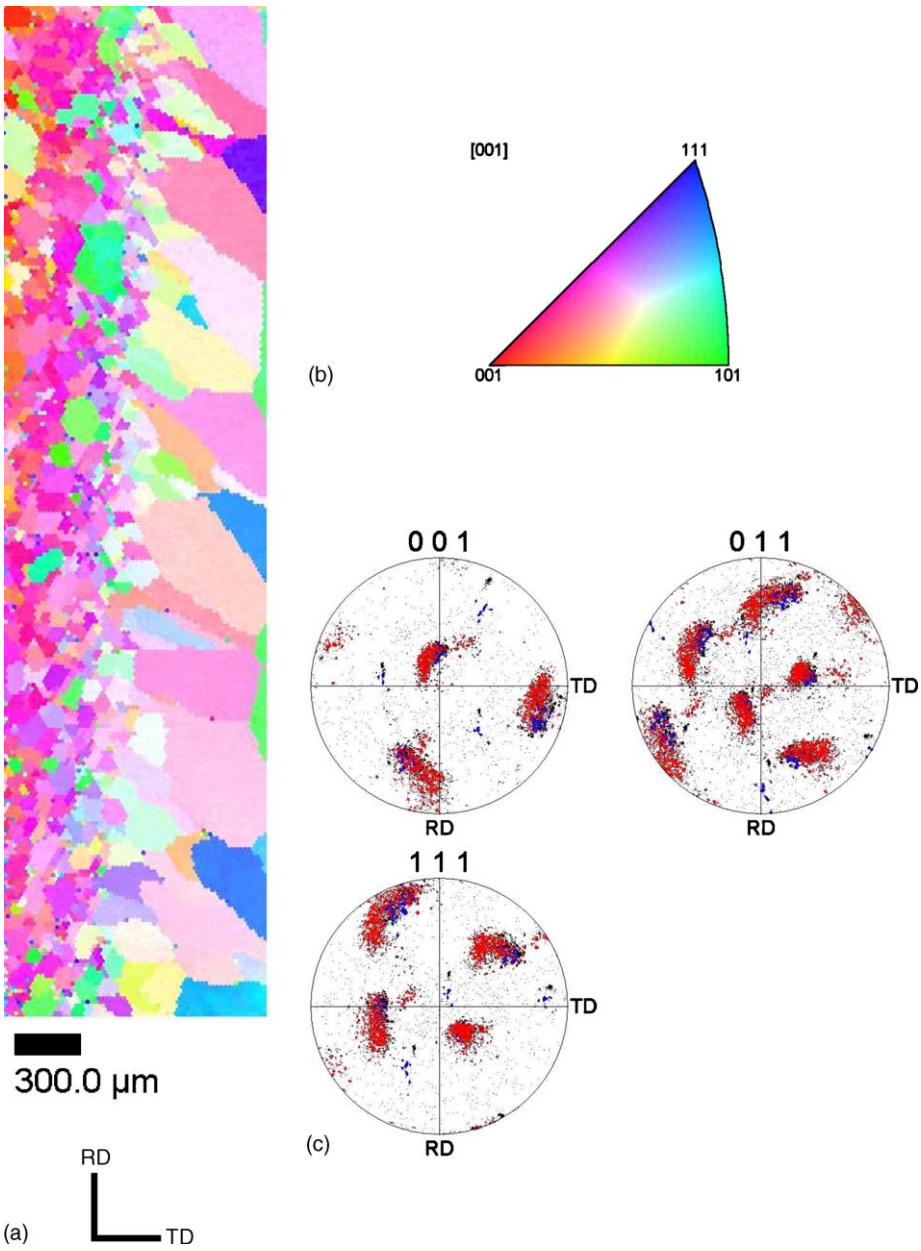

Fig. 5. Orientation image mapping from EBSD data from the region shown in Fig. 4: (a) OIM; (b) unit triangle with color scheme for orientations along the RD; (c) pole figures showing the orientation of fine (left part of the OIM; indicated by red points) and coarse-elongated grains (right part of the OIM; indicated by blue points) in the mapped region.

graph) was found to be $\{0\,0\,1\}\langle 1\,1\,0\rangle$ (rotated cube). The respective pole figures determined from EBSD data are shown in Fig. 8b.

Even in regions where full recrystallization took place there are strong differences in terms of the developed texture in the annealed state. Fig. 9 shows how texture varies within an individual grain. There is a sharp transition dividing two areas of the same micrograph. The region marked by 1 (left part of the micrograph) represents a collection of grains with a slightly elongated morphology with texture centered on $\{1\,1\,1\}\langle u\,v\,w\rangle$. A pronounced orientation spread around TD is evidenced in this region. In the right side of the figure, grains with a more equiaxed morphology are $\{1\,1\,1\}\langle 1\,1\,2\rangle$-oriented.

Another representative example of texture heterogeneity within individual grains is displayed in Fig. 10. Once more a sharp transition between two recrystallized regions within a single grain is present. Grain morphology also varies from one side to another. The OIM referred to this micrograph is shown in Fig. 11. The orientation distribution function (ODF) corresponding to the mapped area reveals the presence of orientations mostly along γ fiber (see ODF section for $\varphi_2 = 45^\circ$). Goss $\{1\,1\,0\}\langle 0\,0\,1\rangle$ and cube $\{1\,0\,0\}\langle 0\,0\,1\rangle$ components are also present, but in a minor extent.

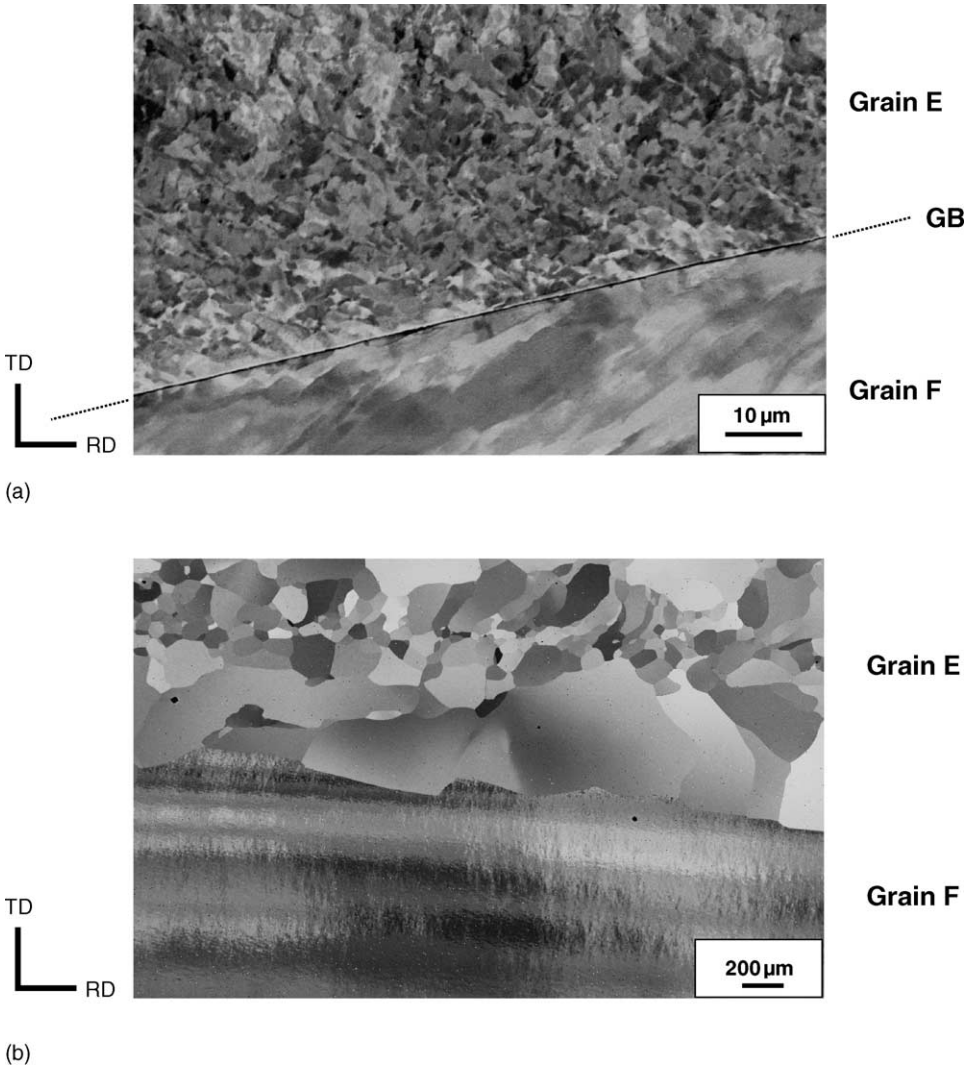

Fig. 6. Longitudinal section of grains E and F: (a) 80% cold rolled; (b) annealed at 1200 °C for 1 h (SEM, BSE).

4. Discussion

The tantalum ingot investigated in this work is a typical oligocrystalline material. EBM and VAR are commonly used to manufacture tantalum ingots. In this regard, understanding the deformation behavior of this type of microstructure and further annealing behavior is essential. In that sense, crystallographic texture plays a decisive role since it influences mechanical properties and further formability of tantalum sheets, especially in the manufacture of deep-drawn parts. There are only a few studies showing the presence of texture gradients in plates processed from EBM- and VAR-Ta [8–10]. These papers report the effects of processing variables on the resulting crystallographic texture of tantalum. These variables included the amount of deformation, grain size, annealing temperature, and the nature of the forming process used to manufacture Ta plates, i.e. direction and amount of forging and/or rolling.

The first point to be addressed in this discussion is the large heterogeneity of the deformation microstructure found in coarse-grained tantalum after cold rolling. In an earlier paper [11], the microstructural heterogeneity of coarse-grained tantalum deformed by cold swaging to large strains was demonstrated. This heterogeneity was associated with orientation effects occurring during grain subdivision. It has been shown that a few grains appeared to deform in a stable manner producing structureless grains or coarse subgrain structures (mosaic-like) in SEM. These grains developed only very low misoriented dislocation structures which are much more susceptible to be softened by recovery than recrystallize. In contrast, the majority of grains split up in strongly misoriented lamellae with high-angle character. These grains provide more favorable nucleation sites for recrystallization.

Orientation effects were also observed during recrystallization of coarse-grained tantalum deformed by cold swaging [12]. Strong differences in terms of the misorientation de-

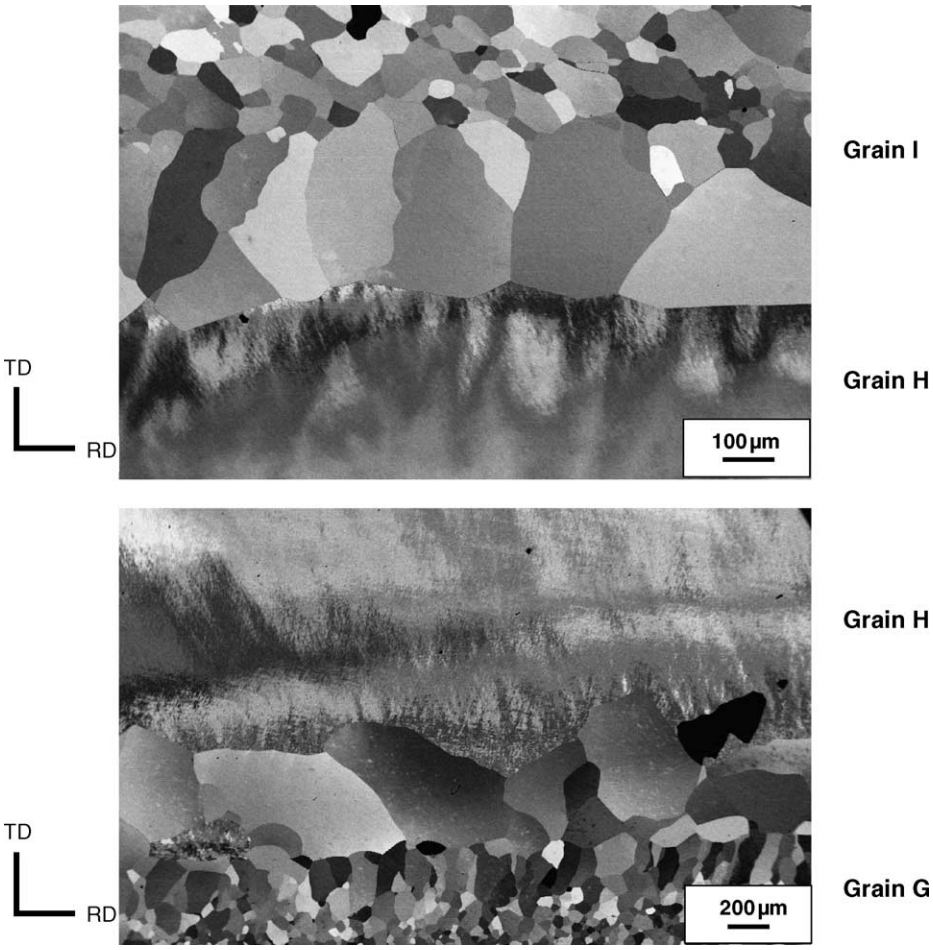

Fig. 7. Longitudinal sections showing three consecutive grains G–H–I in a 80% cold-rolled tantalum sheet followed by annealing at 1200 °C for 1 h (SEM, BSE). Note that recrystallization is absent in grain H.

Table 2
Results of Vickers microhardness testing of selected grains in cold-rolled tantalum and their respective microstructures after annealing at 1200 °C for 1 h

Grain	Reduction (%)	Microhardness (VHN-100 g)	Microstructure after annealing at 1200 °C for 1 h
A	70	97 ± 8	RV
B	70	134 ± 8	RX
C	70	135 ± 21	RX
D	70	112 ± 13	RX
E	80	127 ± 18	RX
F	80	97 ± 9	RV
G	80	122 ± 9	RX
H	80	92 ± 2	RV
I	80	160 ± 6	RX
J	92	175 ± 19	RX
K	92	151 ± 30	RX

RX—recrystallized; RV—recovered.

veloped were observed in two neighboring grains using electron backscattering diffraction (EBSD). The grain with the larger fraction of high angle boundaries recrystallized easily. In contrast, recrystallization was virtually absent in the other grain because of the predominance of boundaries with low angle character. These features are repeated in the rolled material. From the results of microhardness testing (see Table 2) and misorientation distributions shown in Fig. 2, grain B has a much higher stored energy compared to grain A. The presence of many boundaries with high angle character explains why grain B recrystallized with ease and grain A did not.

The presence of large elongated bands parallel to the RD where recrystallization did not occur demands a more detailed discussion. These large bands mark the presence of individual grains and correspond to stable orientations persisting even after large straining, as shown in Fig. 8. They are

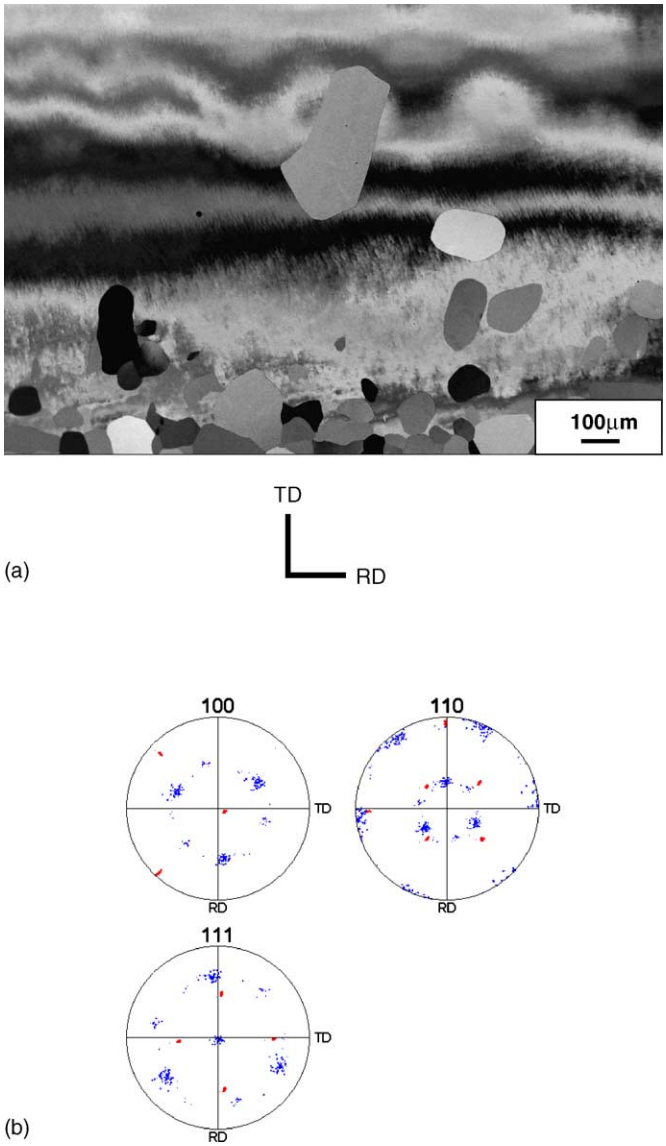

Fig. 8. Micrograph showing the heterogeneous microstructure found in the grain boundary region of a sample 92% cold rolled followed by annealing at 1200 °C for 1 h: (a) general view of the microstructure (SEM, BSE); (b) pole figures corresponding to the recrystallized grains shown in the lower part of the SEM micrograph ($\{1\,1\,1\}\langle 1\,1\,2\rangle$ texture, blue points) and the recovered region ($\{001\}\langle 0\,1\,1\rangle$, red points) shown in the upper part of the SEM micrograph.

found in minor extent even in specimens annealed at 1200 °C for 1 h. The EBSD data shown in this work confirms the presence of orientation effects on recrystallization of the selected tantalum bicrystal as shown in Fig. 2 [6]. Grain A was found to be $\{0\,0\,1\}\langle 1\,1\,0\rangle$-oriented. The rotated cube orientation has a very low Taylor factor which gives rise to low-misoriented regions and hence a very weak tendency to form potential nuclei during recrystallization [13]. The $\{0\,0\,1\}\langle 1\,1\,0\rangle$ (rotated cube) and $\{0\,0\,1\}\langle 1\,0\,0\rangle$ (cube) orientations in Fe–Si single crystals are examples of sluggish orientations in terms of recrystallization [14]. Raabe et al. [15] have reported the occurrence of large recovered areas in rolled and annealed bcc metals attributed to the presence of rotated-cube oriented grains. $(0\,0\,1)[1\,1^{-}\,0]$-oriented tantalum single crystals displayed no recrystallization even after annealing at higher temperatures (1400 °C) [16]. The use of transverse rolling was also reported to promote undesirable rotated cube ($\{0\,0\,1\}\langle 1\,1\,0\rangle$) components in tantalum plates [8,10]. Thus, the large structureless bands appearing in Figs. 4 and 6–8 correspond to recovered grains. These findings are confirmed by microhardness testing taken in structureless bands (grain A, for example) suggesting that recovery was the chief softening mechanism in these grains.

It is very well known that recovery and recrystallization are competing mechanisms. In both cases, the stored energy of deformation is the driving force for the transformation. Assuming that nucleation is relatively uniform, growth of nuclei tend to be faster within grains or regions having higher stored energies. Depending on the annealing temperature, the final microstructure consists of regions where recrystallization takes place faster while within other grains it seems to be slower. This explains the presence of adjacent regions displaying distinct behaviors in terms of recrystallization (volume fraction, texture, and grain size), as demonstrated in Figs. 4 and 6–8.

The recrystallization behavior of cold-rolled tantalum is comparable with the one observed for coarse-grained niobium processed by electron-beam melting. A high-purity coarse-grained niobium bicrystal was 70% cold rolled in multiple passes. Deformation occurred in an inhomogeneous manner in both grains giving rise to a banded structure. In consequence, highly misoriented boundaries were developed in the microstructure in a wide range of misorientations, many reaching about 55°. These boundaries acted as effective nucleation sites for recrystallization [17]. Similarly, the presence of deformation heterogeneities (e.g. deformation bands) or regions of localized deformation in the interior of the grains (see Fig. 3) and in the vicinity of the prior grain boundaries ease the nucleation of new grains at lower annealing temperatures in oligocrystalline tantalum. Considerable evidences supporting these features are found elsewhere [18–20].

The annealed specimens display a band-like structure alternating fully recrystallized, partially recrystallized and recovered regions. This banded microstructure results from the splitting of the majority of the former coarse grains into multitextural components. This peculiar microstructure has been reported for other metals like high-purity coarse-grained aluminum deformed by cold rolling [21]. This inhomogeneous microstructure in the annealed state has been explained in terms of the orientation-dependant mobility of grain boundaries and oriented nucleation concepts. These differences in terms of the rates of static recrystallization and grain size can be related to orientation aspects of growth of nuclei/grains in heavily deformed metals. Our results seem to be in agreement with this proposition, i.e., that of the heterogeneous microstructure of rolled products results from the initial coarse-grained structure. Taking into account orientation effects, it is expected that the growth of nuclei/grains is favored in some

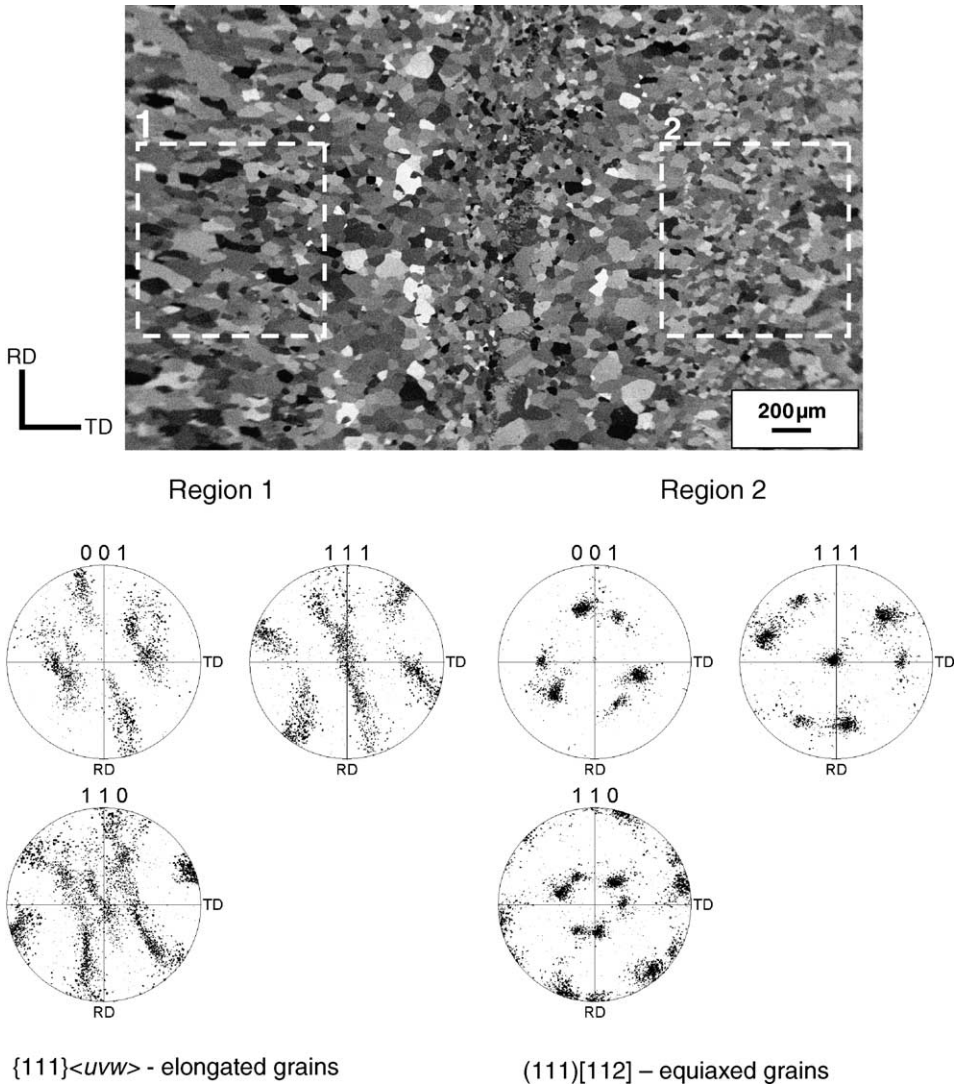

Fig. 9. SEM micrograph showing two adjacent regions within former grain K (92% cold rolled + annealing at 1200 °C for 1 h) where grain size and texture vary from region 1 to region 2 (BSE). Note a sharp transition in the central part of this micrograph.

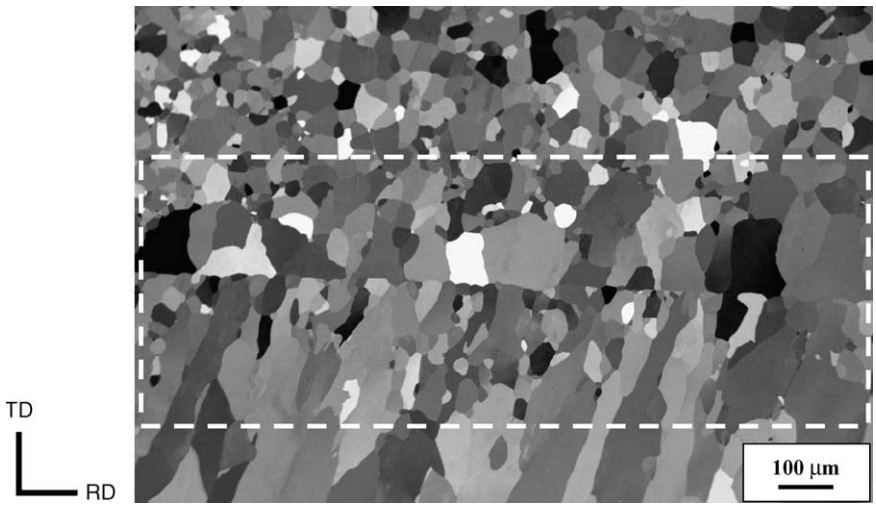

Fig. 10. Detail of a sharp transition dividing two recrystallized regions within former grain G (80% cold rolled + annealing at 900 °C for 1 h). Grain size and morphology vary significantly within the region delimited by this former grain (SEM, BSE).

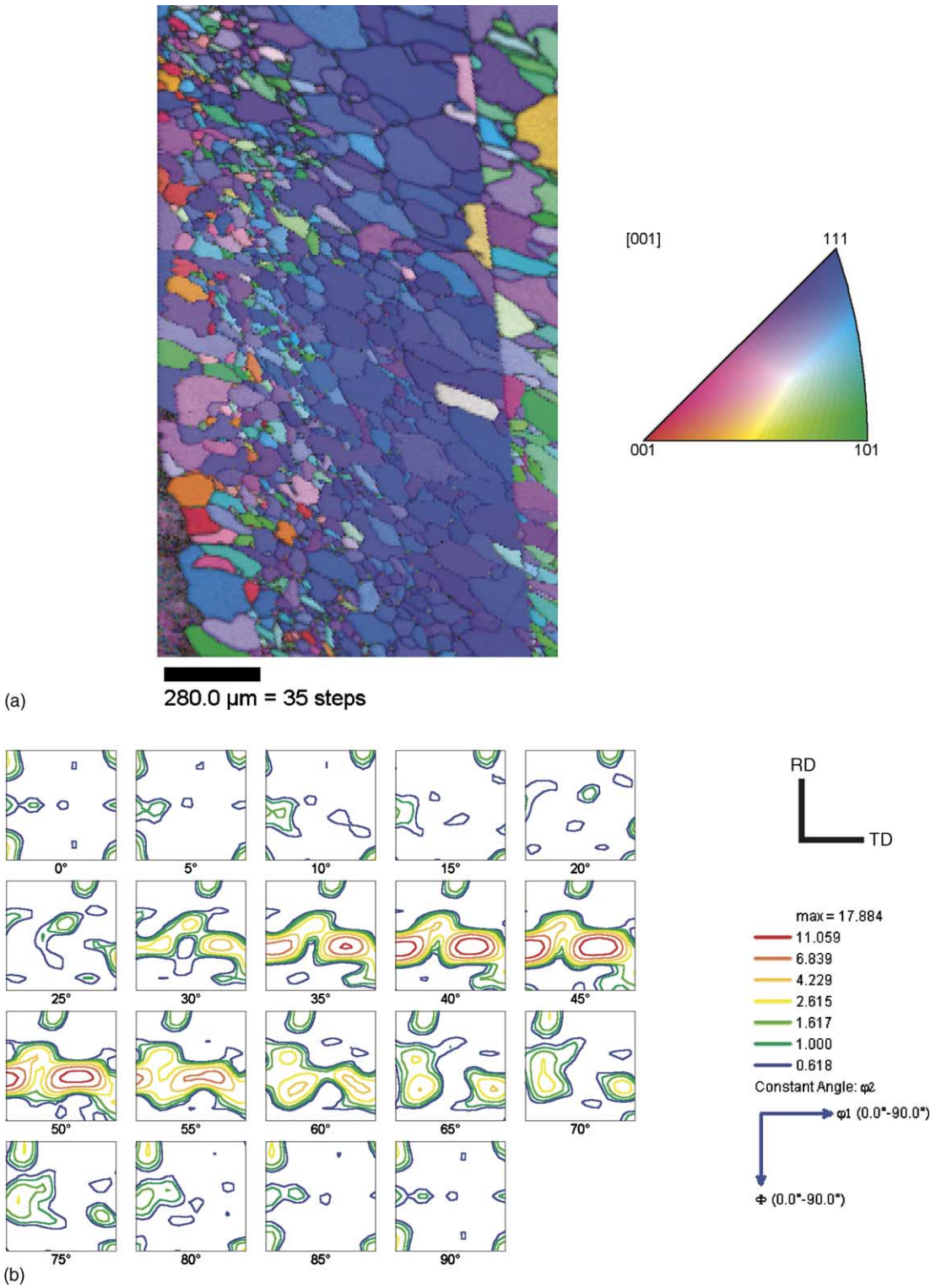

Fig. 11. Orientation image mapping from EBSD data from the region shown in Fig. 10 (dashed rectangle) corresponding to the sharp transition between texture components in former grain G: (a) OIM; (b) ODF showing the texture components and respective intensities found in the mapped region. The γ fiber is predominant followed by weaker Goss $\{1\,1\,0\}\langle 0\,0\,1\rangle$ and cube $\{1\,0\,0\}\langle 0\,0\,1\rangle$ texture components. The unit triangle with color scheme for orientations along the RD is also shown.

cases while in others orientation pinning may affect the nuclei/grain growth rate leading to remarkable differences in terms of grain size as shown in Fig. 11. A detailed discussion about this subject is given in Ref. [22].

Another striking feature observed in the annealed specimens was the presence of coarse grains growing into recovered areas. This is evident in Figs. 4, 6 and 7. Similar features were reported in coarse-grained aluminum [21]. Oriented growth was the explanation proposed by Nes et al. [21] to explain the presence of coarse $\{1\,1\,1\}\langle 1\,1\,0\rangle$-oriented grains growing into the Brass-$\{0\,1\,1\}\langle 2\,1\,1\rangle$ component. In aluminum the high mobility of the $\{1\,1\,1\}$-tilt-boundaries results in a planar growth selection of 40°-$\{1\,1\,1\}$-oriented grains. During primary recrystallization of tantalum, growth selection is the mechanism proposed to explain the disappearance of the rolling texture $\{1\,1\,2\}\langle 1\,1\,0\rangle$ and the corresponding growth of $\{1\,1\,1\}\langle 1\,1\,2\rangle$ texture [23]. These orientations have a 35°-$\langle 1\,1\,0\rangle$ relationship, i.e. close to the 27°-$\langle 1\,1\,0\rangle$-orientation relationship. The 27°-$\langle 1\,1\,0\rangle$-orientation relationship in ferritic steels and b.c.c. refractory metals is characteristic of very mobile high-angle boundaries with Σ19a symmetry, which determines the final texture by a growth selection mechanism [23]. The coarse grains growing into former grain A (Fig. 4) display such morphology probably because they exhibit a noticeable growth advantage and also because of the lack of competing grains in former grain A. The recrystallization texture of the elongated grains is similar to the texture corresponding to the fine-grained structure as shown in Fig. 5. However, these coarse grains display a ∼30°-$\langle 1\,1\,0\rangle$-orientation relationship to the recovered grain A. These observations support the selective growth mechanism for recrystallization in coarse-grained tantalum.

The in-grain and grain-to-grain texture gradients found in this material have to be considered for further processing of tantalum sheets. In addition to a fine-grained structure, a strong γ fiber ($\{1\,1\,1\}\langle u\,v\,w\rangle$, $\{1\,1\,1\}\langle 1\,1\,2\rangle$ or $\{1\,1\,1\}\langle 1\,1\,0\rangle$ texture components) is recommended for further deep drawing of tantalum parts [10]. The γ fiber in b.c.c. refractory metals has a maximum at $\{1\,1\,1\}\langle 1\,1\,2\rangle$ [23]. It comprises orientations where $\{1\,1\,1\}$ planes are parallel to the ND. $\{1\,0\,0\}\langle 0\,v\,w\rangle$ texture components belong to the so-called α fiber and are not suitable for further deep drawing of rolled sheets. The α fiber is usually incomplete and comprises orientations with a common $\langle 1\,1\,0\rangle$-direction parallel to the RD.

Fig. 9 reveals the presence of in-grain texture gradients. EBSD, in this case, is very useful to detect differences in texture in the grain-size scale. This is an advantage on conventional X-ray diffraction techniques used to evaluate crystallographic texture. There is a clear transition from one side to another within the boundary of former grain K. In our view, this has probably to do with the occurrence of deformation banding during fragmentation of coarse-grained materials. Deformation bands are defined as volumes of constant orientation that differ significantly to the orientation(s) found elsewhere within a grain [7,24]. These volumes rotate during grain fragmentation and tend to develop distinct substructures during plastic deformation. Hence, the annealed microstructure shown in Fig. 9 reflects the development of such distinct deformation textures within a grain. Fig. 10 brings another example of texture gradients due to the occurrence of deformation banding within coarse grains. Grain G has a clear boundary dividing two parts of the prior grain. These regions display different recrystallization texture components. This "boundary" is not related to the former grain boundary. Fig. 11 shows that the desirable γ fiber component is predominant in the middle of the OIM scan. Weaker components like Goss $\{1\,1\,0\}\langle 0\,0\,1\rangle$ and cube $\{1\,0\,0\}\langle 0\,0\,1\rangle$ are also present in the right side of the mapped area. Defects caused by inhomogeneous thinning of the sheet during deep drawing are expected to take place in such microstructure.

It must be noted that through-thickness texture gradients were not evaluated in the present paper. Through-thickness texture gradients depend on strain history and were also reported in fine-grained tantalum plates [25]. According to the authors, these gradients could explain the effects of non-uniform microstructures on inhomogeneous plastic behavior of tantalum in rolled products.

5. Conclusions

(a) The static recrystallization in oligocrystalline tantalum deformed by straight cold rolling is strongly dependent on the nature of the deformation microstructure exhibited by individual grains. Orientation effects during grain subdivision are evident in coarse-grained tantalum.
(b) The recrystallization kinetics in EBM-Ta clearly varies from grain to grain. As a result, the microstructure of the annealed specimens is very inhomogeneous and consists predominantly of recrystallized areas with distinct mean grain sizes and a minority of tiny elongated regions softened by recovery. The heterogeneity observed in the annealed microstructure of this coarse-grained material can be predominantly related to orientation effects.
(c) Recrystallization microtexture varies within and from one grain to another. In the rolling plane the dominant texture is the γ fiber ($\{1\,1\,1\}$//ND). The presence of tiny recovered regions in the annealed plate is associated with stable orientations like the rotated cube $\{0\,0\,1\}\langle 1\,1\,0\rangle$, which resist to recrystallization even at high annealing temperatures.

Acknowledgements

Authors are thankful to FAPESP for the financial support (99/11756-0 and 00/12505-5). H.R.Z. Sandim is supported by CNPq (Brazil).

References

[1] S.M. Cardonne, P. Kumar, C.A. Michaluk, H.D. Schwartz, Int. J. Refr. Met. Hard Mater. 13 (1995) 187.
[2] M.F. Hupalo, H.R.Z. Sandim, Mater. Sci. Eng. 318A (2001) 216.
[3] N. Hansen, Metall. Trans. 16A (1985) 2167.
[4] N. Hansen, Mater. Sci. Technol. 6 (1990) 1039.
[5] D.A. Hughes, in: E.N.C. Dalder, T. Grobstein, C.S. Olsen (Eds.), Evolution of Refractory Metals and Alloys, TMS, Pittsburg, 1993, p. 219.
[6] H.R.Z. Sandim, J.P. Martins, A.F. Padilha, Scripta Mater. 45 (2001) 733.
[7] C.S. Lee, B.J. Duggan, R.E. Smallman, Acta Metall. Mater. 41 (1993) 2265.
[8] J.B. Clark, R.K. Garrett Jr., T.L. Jungling, R.A. Vandermeer, C.L. Vold, Metall. Trans. 22A (1991) 2039.
[9] J.B. Clark, R.K. Garrett Jr., T.L. Jungling, R.I. Asfahani, Metall. Trans. 22A (1991) 2959.
[10] J.B. Clark, R.K. Garrett Jr., T.L. Jungling, R.I. Asfahani, Metall. Trans. 23A (1992) 2183.
[11] H.R.Z. Sandim, H.J. McQueen, W. Blum, Scripta Mater. 42 (2000) 151.
[12] H.R.Z. Sandim, A.F. Padilha, V. Randle, W. Blum, Int. J. Refr. Met. Hard Mater. 17 (2000) 431.
[13] D. Raabe, G. Schlenkert, H. Weisshaupt, K. Lücke, Mater. Sci. Technol. 10 (1994) 299.
[14] H. Hu, Trans. AIME 224 (1962) 75.
[15] D. Raabe, F. Roters, V. Marx, Textures Microstruct. 26–27 (1996) 611.
[16] R.A. Vandermeer, W.B. Snyder Jr., Metall. Trans. 10A (1979) 1031.
[17] H.R.Z. Sandim, J.F.C. Lins, A.L. Pinto, A.F. Padilha, Mater. Sci. Eng. A354 (2003) 217.
[18] J.P. Hirth, Metall. Trans. 3 (1972) 3047.
[19] R.D. Doherty, et al., Mater. Sci. Eng. A238 (1997) 219.
[20] J.P. Martins, Dissertation, FAENQUIL, Lorena, Brazil, 2002, 112 pp.
[21] J. Hjelen, R. Ørsund, E. Nes, Acta Metall. Mater. 39 (1991) 1377.
[22] D. Juul Jensen, Acta Metall. Mater. 43 (1995) 4117.
[23] D. Raabe, K. Lücke, Scripta Met. Mater. 27 (1992) 1533.
[24] F.J. Humphreys, M. Hatherly, Recrystallization and Related Annealing Phenomena, Pergamon Press, Oxford, 1995, p. 40.
[25] S.I. Wright, G.T. Gray III, A.D. Rollet, Metall. Trans. 25A (1994) 1025.